Kinetically controlled synthesis of PdNi bimetallic porous nanostructures with enhanced electrocatalytic activity

*Chengzhou Zhu, Dan Wen, Martin Oschatz, Matthias Holzschuh, Wei Liu, Anne-Kristin Herrmann, Frank Simon, Stefan Kaskel, and Alexander Eychmüller**

Dr. C. Zhu, Dr. D. Wen, A.-K. Herrmann, Dr. W. Liu, Prof. A. Eychmüller
Physical Chemistry, TU Dresden, Bergstrasse 66b, 01062 Dresden, Germany
E-mail: alexander.eychmueller@chemie.tu-dresden.de
M. Oschatz, Prof. S. Kaskel
Inorganic Chemistry, TU Dresden Bergstrasse 66, 01062 Dresden, Germany
M. Holzschuh, Dr. F. Simon
Leibniz Institute of Polymer Research Dresden, Hohe Strasse 6, 01069 Dresden, Germany

Keywords: Pd, bimetallic nanomaterials, porous nanostructures, electrocatalysis, fuel cells

Currently, much attention has been paid to the synthesis of shape- and size-controlled noble metal nanomaterials that possess novel physical and chemical properties.[1] Furthermore, the formation of self-assembled architectures is attracting considerable interest and opens up fascinating options for the preparation of new functional nanomaterials.[2] The properties of high surface area, high porosity, and low density in three-dimensional (3D) porous nanoarchitectures lead to promising applications in many fields such as electro-chemical energy storage, catalysts, sensors, and more.[3] To further extend their applications, versatile and reliable synthetic routes have been developed to prepare porous metal nanoarchitectures, ranging from the dealloying[4] and templating,[5] electrochemical synthesis,[6] self-assembly[7] to the direct solvent synthesis approaches.[8] A typical example is that our group has synthesized a series of noble metal-based aerogel using destabilization and direct solvent

synthesis, such as unsupported monometallic,[7, 9] bimetallic[10] and composite aerogels.[11] These noble metal-based aerogels exhibit excellent electrocatalytic performance and hold great promise in fuel cells.

Pd-based nanostructures have attracted tremendous research attention in fuel cells.[12] Compared with Pt-based catalysts, the less expensive and widely available Pd has been exploited as a substitute for Pt in fuel cells in that it can be highly active for the oxidation of a large variety of substrates in an alkaline medium.[13] Recent advances revealed that a rational synthesis of Pd-based bimetallic nanostructures can obviously improve the overall electrocatalytic activities of Pd because of the bimetallic synergistic effect. In addition to noble metals,[14] it is worthwhile to note that non-noble metals, such as Co,[15] Cu,[16] Ni[17] and Sn[18] also have been investigated as substitutes for the noble metals to construct promising Pd-based bimetallic electrocatalysts. Often, however, the strategy for preparing Pd/non-noble metal bimetallic nanostructures requires harsh experimental conditions, is difficult to generalize, and usually limited to complex methods bringing more difficulties in the synthetic process. On this basis, the simultaneous controlling construction of a 3D porous architecture is also expected to provide enormous opportunities for tailoring their properties, and thus enhancing their functions and applications. Thus far developing a facile and general approach to synthesize 3D Pd/non-noble metal porous nanostructures with high electrocatalytic activity has only a limited success and is still a grand challenge for the development of advanced electrocatalysts for fuel cells.

Herein, the kinetically controlled synthesis of a class of 3D Pd/non-noble metal bimetallic nanomaterials with porous nanostructures was reported. Briefly, metal precursors containing H_2PdCl_4 and $NiCl_2$ solution were quickly injected into an aqueous solution of $NaBH_4$ with specific concentration and volume at room temperature. Bimetallic porous nanostructures could be formed within short time in the absence of any capping agent (Figure S1). The final product was obtained after supercritical drying. Moreover, the Pd contents of the final

products could be easily controlled by simply varying the ratio between the Pd and Ni precursors. The compositions of PdNi bimetallic nanostructures, as measured by ICP analysis, were $Pd_{83}Ni_{17}$, $Pd_{72}Ni_{28}$, and $Pd_{53}Ni_{47}$ (the numerical subscripts denote the atomic ratio of the metals), which corresponded to the precursor Pd/Ni molar ratios of 4:1, 2:1, and 1:1, respectively.

The structural features of the PdNi porous nanostructures were investigated by scanning electron microscopy (SEM). Note that the obtained $Pd_{83}Ni_{17}$ porous nanostructures have 3D network-like architectures (**Figure 1** A, B). The highly porous structure and large void space result in an ultralow bulk density of around 0.12 g cm^{-3}, which corresponds to approximately 1/100 of the bulk density of $Pd_{83}Ni_{17}$. Figure 1C and D show transmission electron microscopy (TEM) images of the as-prepared $Pd_{83}Ni_{17}$. Careful observation of this 3D porous nanostructures confirmed that unlike the agglomerated structures, the present $Pd_{83}Ni_{17}$ does not show single nanoparticles separated well from each other but fused irregular nanoparticles with the diameter of between 2 and 10 nm. A high-resolution TEM (HRTEM) was carried out to illustrate the detailed features. As shown in Figure 1E, the crystalline domains containing lattice planes with interplanar distances of about 0.22 nm are assigned to the (111) plane of face centered cubic metallic $Pt_{83}Ni_{17}$, and are widely distributed on the product. Furthermore, High-angle annular dark-field scanning TEM (HAADF-STEM) and energy-dispersive X-ray spectroscopy (EDX) analysis were measured to study the elemental distributions of Pd and Ni in the obtained $Pd_{83}Ni_{17}$. The images in Figure 1F reveal that the elemental distributions are uniform and similar, indicating that Pd and Ni are evenly distributed throughout the nanostructures. Additionally, similar porous nanostructures could also be obtained for both $Pd_{72}Ni_{28}$ (Figure S2A, C) and $Pd_{53}Ni_{47}$ (Figure S2B, D), indicating the change of the composition had no effect on the morphology of the final products. Besides these Pd-based porous nanostructures, monometallic Ni networks (Figure S3) were for the first time fabricated using this facile method, demonstrating the versatility of this method and holding

great promise in their practical applications. Although gained via different synthetic processes, the morphology of the products are similar to the monometallic and bimetallic aerogels reported previously.[7, 9] Both of them are bound up with the process of fusion of the obtained nanoparticles. However, the shape of the fused units varies due to different growth mechanisms. On the basis of the aforementioned observation and analyses, we can come to the conclusion that the rapid fusion and growth of bare bimetal nuclei takes place during the kinetically controlled sodium borohydride reduction process which can induce the formation of the 3D porous network instantaneously.[19] It is proven that metal nanoparticles instead of 3D porous nanostructures are rapidly formed when the concentration of the metal precursors and the reducing agent is low.

The crystal structures of the bimetallic PdNi and the monometallic Pd and Ni porous nanostructures were characterized and **Figure 2A** gives their X-ray powder diffraction (XRD) patterns. For the series of the PdNi nanostructures, besides similar distinct peaks for Pd, there also exist another two small peaks at 2 θ values of about 33.1 and 59.3°, which can be attributed to the $Ni(OH)_2$ (100) and (110) facets, respectively.[20] In addition, their intensities increase with the Ni content. These two peaks were also confirmed at the same position for porous Ni nanostructures with the exception of other peaks being ascribed to the metallic state of Ni. Compared with Pd, no significant shift is observed for all the PdNi nanostructures, which suggests that Pd and Ni do not alloy well with this preparation method.[20-21]

X-ray photoelectron spectroscopy (XPS) analysis (Figure S4) shows that the Pd/Ni atomic ratio on the surface of $Pd_{83}Ni_{17}$ was 2.6, indicating that the outer surface of these nanostructures are enriched with Ni, as compared with their bulk compositions. Due to the difference in the reduction potential between Pd^{2+} and Ni^{2+}, the formation of the final product might be initiated by a Pd enriched inner and then Ni-enriched surface. The Pd3d XPS spectra of the $Pd_{83}Ni_{17}$ nanostructures are shown in Figure 2B. Apparently, the spectrum indicates the existence of the metallic state of Pd (78.6%) as well as small part of Pd^{II}. Also, a close

inspection of the XPS Pd3d spectra shows that a slight shift of the Pd 3d peak towards lower binding energy increased with the increasing content of Ni (Figure 2C), which could be ascribed to the modification of the electronic structure of Pd by a slight electron transfer from Ni to Pd. This change may modify the electrocatalytic activity of Pd in the methanol electrooxidation process. With regard to Ni, the Ni2p spectrum of the $Pd_{83}Ni_{17}$ shows a complicated structure by the presence of high binding energy satellite peaks adjacent to the main peaks (Figure 2D), which can be attributed to multi-electron excitations. Taking the shake-up peaks into account, the Ni2p3/2 peak spectra are deconvoluted into four peaks at 852.7, 853.8, 855.6 and 857.3 eV, corresponding to metallic Ni, NiO, $Ni(OH)_2$ and NiOOH, respectively,[20a,22] the corresponding XPS area ratios are 11.34, 4.81, 53.83, and 30.02. The XPS area ratios of the chemical states of the Ni species for all the PdNi porous nanostructures are shown in Figure S5 and Table S1. It can be seen that the Ni species are mainly comprised of $Ni(OH)_2$ and NiOOH for all the samples.

In addition to the component and structure analysis, N_2 physisorption isothermal analysis was also conducted to further investigate their surface area and porosity. As shown in **Figure 3A**, the isotherms recorded for all samples are similar in shape regardless of the composition and mainly show a type II behavior with some resemblance to a type IV curve, indicating the typical porous characteristic of the products. Isotherms with a large uptake and no plateau appeared at high relative pressures which proves the presence of macropores inside these nanomaterials. The pore size distribution of these porous nanostructures was assessed (Figure 3B). Besides macropores, all the tested aerogels show the presence of a broad range of pores from micropores (<2 nm) to mesopores (2–35 nm). This broad pore distribution corresponding to a continuous micropore to macropore structure was created by the 3D assembly of the fused nanostructures, which are in good accordance with the results from SEM and TEM characterizations. Mesopores and macropores dominated the porosity of these materials in comparison to micropores according to the pore volume analysis (Figure3B and

Table S2). The specific surface area as estimated from the BET plot is 29.8, 32.1 and 58.9 m^2 g^{-1} for the $Pd_{83}Ni_{17}$, $Pd_{72}Ni_{28}$ and $Pd_{53}Ni_{47}$, respectively. The surface areas of the PdNi are comparable with those of noble metal nanosponges[19] and some bimetallic aerogels.[7] These hierarchical porous nanostructures are without doubt of great advantage for the transport of analytes or reactants and thus greatly enhance their applications as sensors and in catalysis.

The electrocatalytic performance of the PdNi was further examined by choosing methanol as a model molecule and comparing with that of a commercial Pd/C. According to the typical cyclic voltammograms (CVs) in N_2-saturated 0.5 M NaOH (Figure S6A), it is observed that the reduction peak potentials of the PdNi were lower than that of Pd because of the introduction of Ni. The calculated electrochemically active surface areas (ECSA) were 13.4, 37.5, 38.3, 40.1 and 54.9 m^2 g^{-1} for the Pd, $Pd_{83}Ni_{17}$, $Pd_{72}Ni_{28}$, $Pd_{53}Ni_{47}$ and Pd/C, respectively. This indicated that the PdNi porous nanostructures had higher ECSA values compared to Pd, which would probably enhance the active sites for the electrooxidation reaction of methanol. The electrocatalytic activities of these different kinds of catalysts toward methanol oxidation were investigated through cyclic voltammetry (**Figure 4A**). Of the three kinds of PdNi investigated, $Pd_{83}Ni_{17}$ possessed the highest activity and displayed a less positive anodic onset potential and high mass current density. In detail, the peak of current density of the $Pd_{83}Ni_{17}$ (1.11 A mg_{Pd}^{-1}) was 1.96 and 1.26 times higher than those of the $Pd_{72}Ni_{28}$ (0.56 A mg_{Pd}^{-1}) and $Pd_{53}Ni_{47}$ (0.87 A mg_{Pd}^{-1}), respectively. $Pd_{83}Ni_{17}$ also possessed the lowest onset potential at about −0.51 V, which was more negative than that of the $Pd_{72}Ni_{28}$ (−0.50 V) and $Pd_{53}Ni_{47}$ catalysts (−0.49 V). It is well known that the ratio of forward (I_f) to backward (I_b) peak current (I_f/I_b) can be used to evaluate the catalyst tolerance to the intermediate carbonaceous species accumulated on the electrode surface. The I_f/I_b on $Pd_{83}Ni_{17}$ is 1.27 and 2.36 times as large as that on $Pd_{53}Ni_{47}$ and $Pd_{72}Ni_{28}$, respectively, which suggests that $Pd_{83}Ni_{17}$ has less carbonaceous accumulation and hence is much more tolerant towards CO poisoning. We speculate that this composition dependent electrocatalytic activity could be ascribed to

structural and compositional differences. Among them, $Pd_{83}Ni_{17}$ provided the optimum balance between active Pd and Ni sites on the surface of the nanostructures, inducing the high electrochemical performance. As expected, in comparison to single Pd and commercial Pd/C, the optimized $Pd_{83}Ni_{17}$ afforded the preeminent electroactivity with high current density, suggesting the crucial role of the Ni in the electrocatalysis.

Similarly, $Pd_{83}Ni_{17}$ has a higher current density at both the start and the end of the chronoamperometric test (Figure 4B). However, compared to $Pd_{72}Ni_{28}$ and $Pd_{53}Ni_{47}$, $Pd_{83}Ni_{17}$ resulted in poor long-term stability. This may be caused by the Ni content within electrocatalyst surface and the reduced stability of Ni. A detailed investigation on improving the stability of PdNi is still underway. A change of the ECSA of $Pd_{83}Ni_{17}$ was detected using successive electrochemical scans from -1.0 V to 0.35 V in N_2-saturated alkaline solution at room temperature (Figure S6B). After 100 cycles, $Pd_{83}Ni_{17}$ had lost 28.83% of the Pd initial ECSA, while the degradation of the ETEK Pd/C catalyst was quite severe, with 60.89% loss of the initial ECSA. These results suggest that by the combination with Ni, the structure stabilities of PdNi are also greatly enhanced. According to the discussion mentioned above, the enhanced electrochemical response for the $Pd_{83}Ni_{17}$ could be ascribed to the following aspects. First, the Ni surface sites can allow the facile formation of oxygenated species to oxidize the dissociative intermediates produced on nearby Pd sites to facilitate the elimination of the poisoning effect of CO on Pd surfaces.[21] The Ni hydroxide and oxide can act as promoters to enhance their electrochemical performance.[23] Also, the change in the electronic properties of Pd and the center of the d-band because of the coordination of Ni plays a key role in the enhanced methanol oxidation.[24] Additionally, the high electrocatalytic activity of the PdNi can also be ascribed to the 3D porous architecture with a high BET surface area and a clean surface, which favour the exposure of catalytic active sites and the transport and diffusion of the reactants.

Furthermore, an appealing advantage in this work is that the synthesis strategy can be applied to the synthesis of PdCo (Figure S7) and other noble metal/nonprecious metal porous nanostructures with controlled composition. This class of bimetallic porous nanostructures with geometrically favorable factors as well as their synergistic effects offer very attractive prospects and could be extended to the applications in different fields.

In summary, we have presented a facile and general strategy for the kinetically controlled synthesis of a series of 3D Pd/non-noble metal bimetallic porous nanostructures in aqueous solution at room temperature. The obtained PdNi porous nanostructures are composed of 3D networks and display very high surface areas and large porosity. On the one hand, the introduction of the non-noble metal here can effectively reduce the cost of the catalyst, which is favorable for their commercialization. On the other hand, due to their porous nanostructures, their clean surface as well as the synergistic effects between their compositions, the as-prepared PdNi exhibited greatly enhanced activity and stability towards methanol electrooxidation in an alkaline medium. Because of the convenient preparation, the large-scale production and the well-defined porous nanostructures, it is reasonable to believe that this kind of Pd-based porous nanostructure is very promising as a new class of catalysts in fuel cells and other electrochemical energy systems.

Supporting Information
Supporting Information is available from the Wiley Online Library or from the author.

Acknowledgements
This work was supported by the Alexander von Humboldt Foundation. Work on metal aerogel based electrocatalysts is also funded by the EU through the ERC Advanced Grant AEROCAT. We thank Susanne Goldberg for the SEM measurements.

[1] a) L. Wang, Y. Yamauchi, *J. Am. Chem. Soc.* **2009**, *131*, 9152; b) C. Zhu, S. Guo, S. Dong, *Adv. Mater.* **2012**, *24*, 2326.

[2] a) F. J. Heiligtag, M. Niederberger, *Mater. Today* **2013**, *16*, 262; b) B. C. Tappan, S. A. Steiner, E. P. Luther, *Angew. Chem., Int. Ed.* **2010**, *49*, 4544.

[3] a) K. G. S. Ranmohotti, X. Gao, I. U. Arachchige, *Chem. Mater.* **2013**, *25*, 3528; b) C. Xu, L. Wang, R. Wang, K. Wang, Y. Zhang, F. Tian, Y. Ding, *Adv. Mater.* **2009**, *21*, 2165; c) A. Walcarius, *Chem. Soc. Rev.* **2013**, *42*, 4098.

[4] Z. Qi, J. Weissmueller, *ACS Nano* **2013**, *7*, 5948.

[5] H. J. Shin, R. Ryoo, Z. Liu, O. Terasaki, *J. Am. Chem. Soc.* **2001**, *123*, 1246.

[6] L.-X. Ding, A.-L. Wang, G.-R. Li, Z.-Q. Liu, W.-X. Zhao, C.-Y. Su, Y.-X. Tong, *J. Am. Chem. Soc.* **2012**, *134*, 5730.

[7] N. C. Bigall, A.-K. Herrmann, M. Vogel, M. Rose, P. Simon, W. Carrillo-Cabrera, D. Dorfs, S. Kaskel, N. Gaponik, A. Eychmüller, *Angew. Chem., Int. Ed.* **2009**, *48*, 9731.

[8] a) X. Liu, G. Fu, Y. Chen, Y. Tang, P. She, T. Lu, *Chem. Eur. J.* **2014**, *20*, 585-590; b) C. Zhu, S. Guo, S. Dong, *Chem. Eur. J.* **2013**, *19*, 1104; c) Y. Xu, S. Hou, Y. Liu, Y. Zhang, H. Wang, B. Zhang, *Chem. Commun.* **2012**, *48*, 2665.

[9] W. Liu, A.-K. Herrmann, D. Geiger, L. Borchardt, F. Simon, S. Kaskel, N. Gaponik, A. Eychmüller, *Angew. Chem., Int. Ed.* **2012**, *51*, 5743.

[10] a) W. Liu, A.-K. Herrmann, D. Geiger, L. Borchardt, F. Simon, S. Kaskel, N. Gaponik, A. Eychmüller, *Angew. Chem., Int. Ed.* **2012**, *51*, 5743; b) A.-K. Herrmann, P. Formanek, L. Borchardt, M. Klose, L. Giebeler, J. Eckert, S. Kaskel, N. Gaponik, A. Eychmüller, *Chem. Mater.* **2014**, *26*, 1074.

[11] V. Lesnyak, A. Wolf, A. Dubavik, L. Borchardt, S. V. Voitekhovich, N. Gaponik, S. Kaskel, A. Eychmüller, *J. Am. Chem. Soc.* **2011**, *133*, 13413.

[12] C. Bianchini, P. K. Shen, *Chem. Rev.* **2009**, *109*, 4183.

[13] a) S. Guo, S. Dong, E. Wang, *Energy Environ. Sci.* **2010**, *3*, 1307; b) Y.-W. Lee, A. R. Ko, S.-B. Han, H.-S. Kim, D.-Y. Kim, S.-J. Kim, K.-W. Park, *Chem. Commun.* **2010**, *46*, 9241.

[14] a) C.-H. Cui, J.-W. Yu, H.-H. Li, M.-R. Gao, H.-W. Liang, S.-H. Yu, *ACS Nano* **2011**, *5*, 4211; b) Y. Liu, M. Chi, V. Mazumder, K. L. More, S. Soled, J. D. Henao, S. Sun, *Chem. Mater.* **2011**, *23*, 4199.

[15] C. Xu, Y. Liu, H. Zhang, H. Geng, *Chem. Asian J.* **2013**, *8*, 2721.

[16] C. X. Xu, A. H. Liu, H. J. Qiu, Y. Q. Liu, *Electrochem. Commun.* **2011**, *13*, 766.

[17] T. Maiyalagan, K. Scott, *J. Power Sources* **2010**, *195*, 5246.

[18] L.-X. Ding, A.-L. Wang, Y.-N. Ou, Q. Li, R. Guo, W.-X. Zhao, Y.-X. Tong, G.-R. Li, *Sci. Rep.* **2013**, *3*, 1181.

[19] K. S. Krishna, C. S. S. Sandeep, R. Philip, M. Eswaramoorthy, *ACS Nano* **2010**, *4*, 2681.

[20] a) S. Y. Shen, T. S. Zhao, J. B. Xu, Y. S. Li, *J. Power Sources* **2010**, *195*, 1001; b) Z. Zhang, L. Xin, K. Sun, W. Li, *Int. J. Hydrogen Energy* **2011**, *36*, 12686.

[21] F. Zhu, G. Ma, Z. Bai, R. Hang, B. Tang, Z. Zhang, X. Wang, *J. Power Sources* **2013**, *242*, 610.

[22] K.-W. Park, J.-H. Choi, B.-K. Kwon, S.-A. Lee, Y.-E. Sung, H.-Y. Ha, S.-A. Hong, H. Kim, A. Wieckowski, *J. Phys. Chem. B* **2002**, *106*, 1869.

[23] a) P. K. Shen, C. W. Xu, R. Zeng, Y. L. Liu, *Electrochem. Solid-State Lett.* **2006**, *9*, A39; b) K.-W. Park, J.-H. Choi, Y.-E. Sung, *J. Phys. Chem. B* **2003**, *107*, 5851.

[24] Z. Yin, W. Zhou, Y. Gao, D. Ma, C. J. Kiely, X. Bao, *Chem. Eur. J.* **2012**, *18*, 4887.

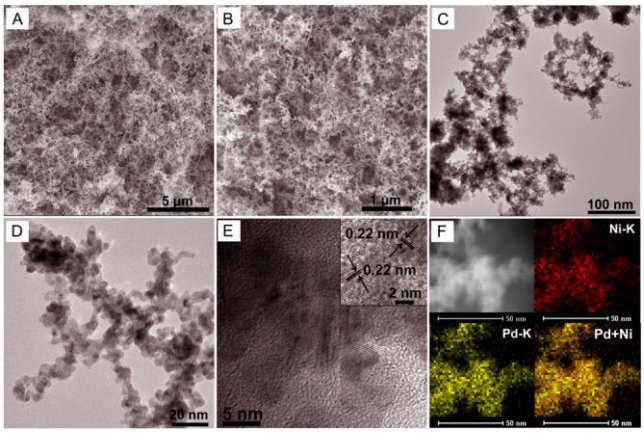

Figure 1. SEM (A, B) and TEM (C, D) images of the $Pd_{83}Ni_{17}$ porous nanostructures. HRTEM (E) and HAADF-STEM-EDX mapping images (F) of $Pd_{83}Ni_{17}$.

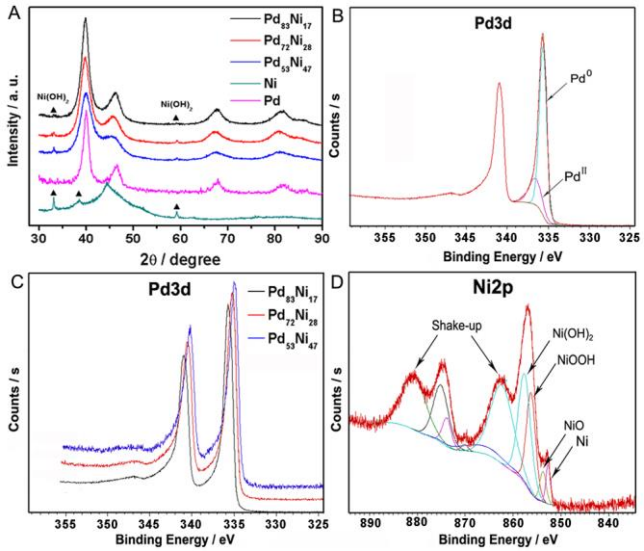

Figure 2. (A) XRD patterns of the bimetallic PdNi and monometallic Pd and Ni porous nanostructures. High resolution Pd3d (B) and Ni2p (D) XPS spectra of the $Pd_{83}Ni_{17}$ nanostructures. (C) High-resolution Pd3d XPS spectra for different PdNi nanostructures.

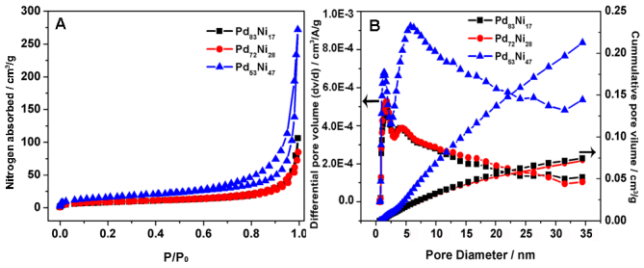

Figure 3. N_2 physisorption isotherms (A), pore size distribution and the corresponding cumulative pore volumes (B) for the $Pd_{83}Ni_{17}$, $Pd_{72}Ni_{28}$, and $Pd_{53}Ni_{47}$.

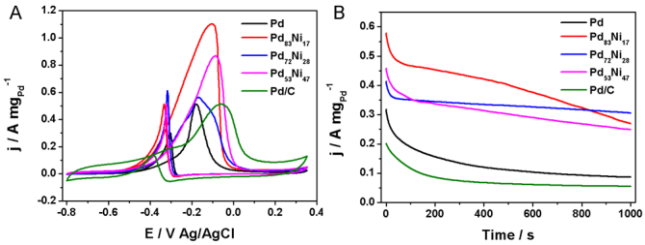

Figure 4. (A) CVs of PdNi with different compositions, Pd and commercial Pd/C electrodes in aqueous 1 M KOH + 1 M methanol solution at a scan rate of 50 mV/s. (B) Current density–time curves of PdNi with different compositions, Pd and commercial Pd/C electrodes in aqueous 1 M KOH+1 M methanol solution at -0.2 V.

A class of 3D PdNi bimetallic nanomaterials with porous nanostructures is synthesized using a facile and versatile approach at room temperature. Due to their porous nanostructures, their clean surfaces as well as the synergistic effect between their compositions, the as-prepared PdNi exhibit greatly enhanced activity and stability towards methanol electrooxidation in an alkaline medium, holding great promise in fuel cells.

Keyword

Chengzhou Zhu, Dan Wen, Martin Oschatz, Matthias Holzschuh, Wei Liu, Anne-Kristin Herrmann, Frank Simon, Stefan Kaskel, and Alexander Eychmüller*

Kinetically controlled synthesis of PdNi bimetallic porous nanostructures with enhanced electrocatalytic activity

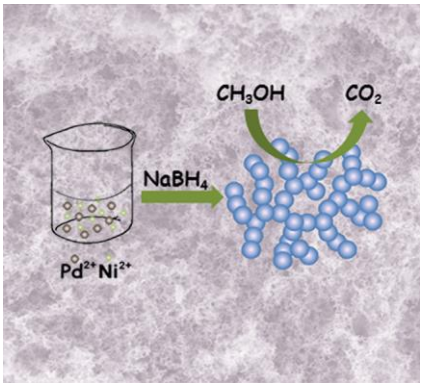

Supporting Information

Kinetically controlled synthesis of PdNi bimetallic porous nanostructures with enhanced electrocatalytic activity

*Chengzhou Zhu, Dan Wen, Martin Oschatz, Matthias Holzschuh, Wei Liu, Anne-Kristin Herrmann, Frank Simon, Stefan Kaskel, and Alexander Eychmüller**

EXPERIMENTAL SECTION

Chemicals: $PdCl_2$, $NiCl_2.6H_2O$ and $CoCl_2.6H_2O$ were purchased from Sigma and used as received without further purification. Commercial Pd/C catalyst was purchased from Alfa Aesar. $NaBH_4$ were obtained from Aldrich. Unless otherwise stated, other reagents were of analytical grade and were used as received. All aqueous solutions were prepared with ultrapure water (>18 MΩ) from a Milli-Q Plus system (Millipore).

Apparatus: Transmission electron microscopy (TEM) measurements were made on a Zeiss Libra. High-resolution TEM (HRTEM) images, High-angle annular dark-field scanning TEM (HAADF-STEM) and energy-dispersive X-ray spectroscopy (EDX) measurements were obtained with a FEI Tecnai G2 F20 S-TWIN operating at 200 kV. X-ray powder diffraction (XRD) was carried out on Siemens D5000 X-ray diffractometer using Cu Kα (1.5406 Å) radiation. Scanning electron microscopy (SEM) was performed on a Zeiss DSM 982 Gemini instrument. X-ray photoelectron spectroscopy (XPS) studies were carried out by means of an AXIS ULTRA photoelectron spectrometer (KRATOS ANALYTICAL, Manchester, England). Inductively coupled plasma optical emission spectroscopy (ICP-OES) was carried out on Perkin-Elmer Optima 7000DV optical emission spectrometer. Nitrogen physisorption isotherms were measured at 77 K on a Quantachrome Autosorb 1 instrument. Prior to the measurement, the samples were degassed in vacuum at 323 K for 24 h. The specific surface area was calculated by using multipoint Brunauer-Emmett-Teller (BET) equation ($0.05<P/P_0<0.2$), and the pore size distribution was determined from the isotherm using

quenched solid density functional theory (QSDFT) equilibrium model based on a slit shaped pore geometry. Electrochemical experiments (Cyclic voltammetry and Chronoamperometry) were performed on an Autolab electrochemical system. A conventional three electrode cell was used, including an Ag/AgCl (3 M NaCl) electrode as reference electrode, a platinum foil as counter electrode, and the modified glassy carbon electrode (GCE, 3 mm in diameter) as working electrode.

Preparation of PdNi bimetallic porous nanostructures. PdNi porous nanostructures were synthesized via a simple method. In a typical synthesis, 5 mL of the metal precursors containing 4.0 mL H_2PdCl_4 (0.1 M) solution and 1.0 mL $NiCl_2$ (0.1 M) solution was quickly injected into 25 mL of an aqueous solution of 0.1 M $NaBH_4$ with stirring. Bimetallic porous nanostructures could be formed within 5 min accompanying by the release of hydrogen. To avoid the collapse and preserve their original morphology, the product was dried supercritically using a critical point dryer, 13200J-AB from SPI Supplies. The final product was obtained for further use. Furthermore, we varied the mole ratios of Pd and Ni sources in the precursor solutions to prepare PdNi porous nanostructures with various mole ratios. As such, the monometallic Pd, Ni and bimetallic PdCo porous nanostructures with various compositions could be also obtained through the same way mentioned above.

Electrocatalytic experiments. Prior to the surface coating, the GCE was polished carefully with 1.0, 0.3 and 0.05 μm alumina powder, respectively, and rinsed with deionized water, followed by sonicated in acetone and doubly distilled water successively. Then, the electrode was allowed to dry under nitrogen. For methanol oxidation reactions, 5 μL of PdNi or Pd/C E-TEK catalyst aqueous solution was dropped on the surface of GCE and dried. The loading of Pd on the GCE was limited to 70.42 μg cm^{-2}. Then, 5 μL of Nafion (0.2 %) was placed on the surface of the above materials modified GCE and dried before electrochemical experiments.

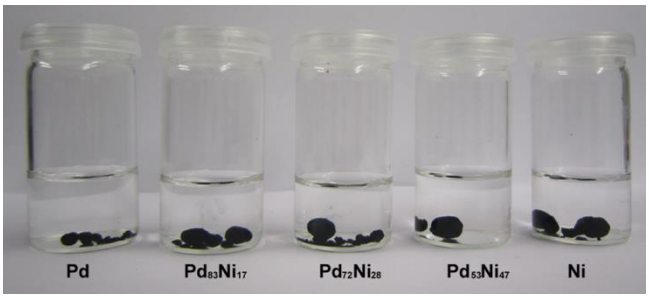

Figure S1. Digital photographs of the bimetallic PdNi, monometallic Pd and Ni nanostructures before supercritical dry.

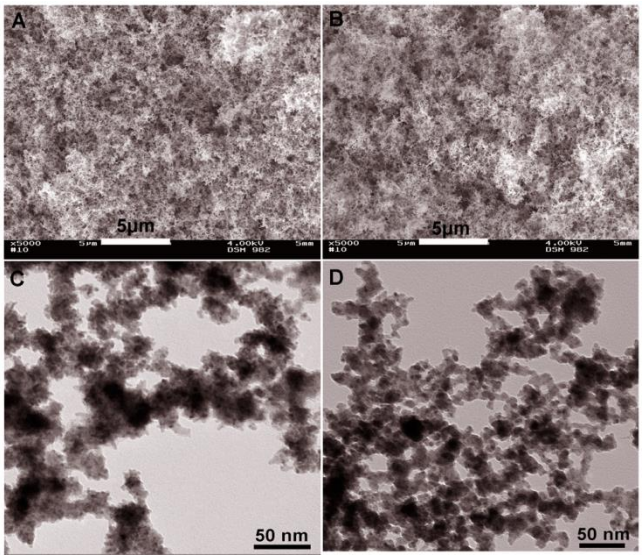

Figure S2. SEM (A, B) and TEM (C, D) images of $Pd_{72}Ni_{28}$ (A, C) and $Pd_{53}Ni_{47}$ (B, D).

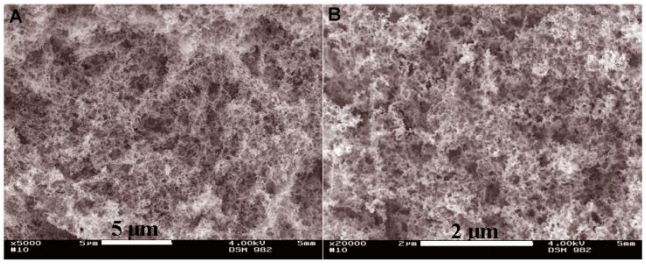

Figure S3. SEM images of Ni porous nanostructures.

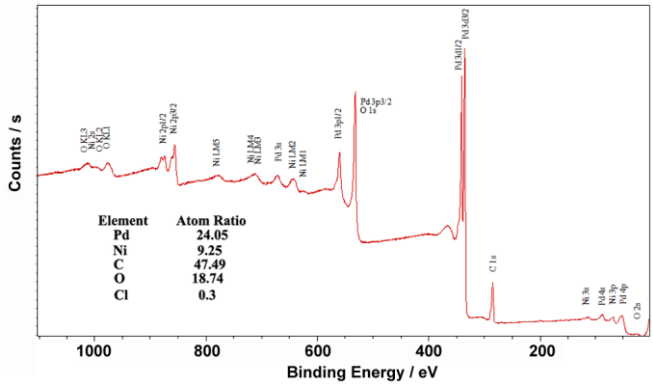

Figure S4. XPS spectra of $Pd_{83}Ni_{17}$ nanostructures.

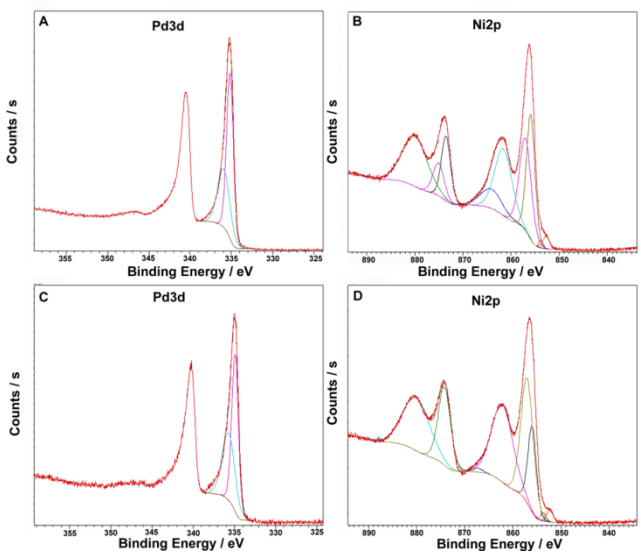

Figure S5. High-resolution Pd 3d (A, C) and Ni 2p (B, D) XPS spectra of the $Pd_{72}Ni_{28}$ (A, B) and $Pd_{53}Ni_{47}$ (C, D) porous nanostructures.

Table S1. Molar ratio of Pd/Ni and percentage of compositions in the PdNi porous nanostructures obtained according to XPS.

Samples	Pd/Ni (%)	Pd/PdO (%)	Ni/NiO/NiOOH/$Ni(OH)_2$ (%)
$Pd_{83}Ni_{17}$	72/28	78.6/21.4	6.57/7.27/34.90/51.25
$Pd_{72}Ni_{28}$	38/62	61.5/38.5	3.65/1.44/46.77/48.13
$Pd_{53}Ni_{47}$	23/77	55.4/44.6	3.23/1.82/30.39/64.56

Table S2. Surface area and porosity of the obtained PdNi nanostructures obtained from N_2 physisorption isothermal analyses.

Samples	BET surface area [m^2/g]	Pore volume [cm^3/g]	Micropore volume [cm^3/g]
$Pd_{83}Ni_{17}$	29.8	0.164	0.0050
$Pd_{72}Ni_{28}$	32.1	0.132	0.0055
$Pd_{53}Ni_{47}$	58.9	0.421	0.0072

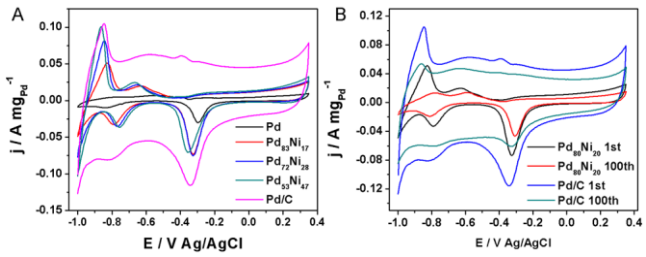

Figure S6. (A) CVs of PdNi with different compositions, Pd and commercial Pd/C in N_2-saturated NaOH solution. (B) CVs of $Pd_{83}Ni_{17}$ and E-TEK Pd/C in N_2 saturated NaOH solution (0.5 M) before and after 100 potential cycles at a scan rate of 50 mV/s.

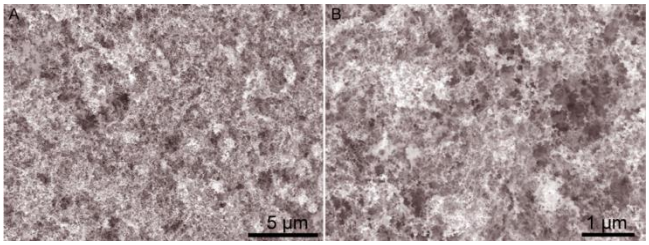

Figure S7. SEM images of the obtained PdCo porous nanostructures.